Applied Physics Letters

Simultaneous single-peak and narrowband thermal emission enabled by hybrid metal-polar dielectric structures

Cite as: Appl. Phys. Lett. **115**, 093505 (2019); https://doi.org/10.1063/1.5100938
Submitted: 22 April 2019 . Accepted: 16 August 2019 . Published Online: 28 August 2019

Lu Cai, Qiang Li, Jianbo Yu, Hao Luo, Kaikai Du, and Min Qiu

Applied Physics Letters ARTICLE scitation.org/journal/apl

Simultaneous single-peak and narrowband thermal emission enabled by hybrid metal-polar dielectric structures

Cite as: Appl. Phys. Lett. **115**, 093505 (2019); doi: 10.1063/1.5100938
Submitted: 22 April 2019 · Accepted: 16 August 2019 ·
Published Online: 28 August 2019

Lu Cai,[1] Qiang Li,[1,a)] Jianbo Yu,[1] Hao Luo,[1] Kaikai Du,[1] and Min Qiu[2,3]

AFFILIATIONS

[1]State Key Laboratory of Modern Optical Instrumentation, College of Optical Science and Engineering, Zhejiang University, Hangzhou 310027, China
[2]Key Laboratory of 3D Micro/Nano Fabrication and Characterization of Zhejiang Province, School of Engineering, Westlake University, 18 Shilongshan Road, Hangzhou 310024, China
[3]Institute of Advanced Technology, Westlake Institute for Advanced Study, 18 Shilongshan Road, Hangzhou 310024, China

[a)]Email: qiangli@zju.edu.cn

ABSTRACT

Simultaneous single-peak and narrowband thermal emitters with the merits of a simple configuration and ease-of-fabrication provide a path to enhance the energy utilization efficiency while they remain a challenge. Here, we demonstrate simultaneous single-peak and narrowband thermal emission by hybridizing metal microstructures with polar dielectric substrates. The metal provides single-peak emission in a broad spectrum range and the polar dielectric assists narrowband operation. The measured peak emissivity of the single-peak transverse-magnetic-polarized emission is 0.94 with a quality factor of 19 at the wavelength of 11.2 μm, and the emission at all other wavelengths from 2.5 μm to 25 μm is significantly suppressed. The utilization of the refractory material (molybdenum) provides further possibility for such a device to operate at temperatures up to 600 °C. These simultaneous single-peak and narrowband thermal emitters suggest avenues for numerous energy-efficient applications including gas sensing, thermal sources, and thermophotovoltaics.

Mid-infrared thermal emitters are essential for numerous applications, including radiative cooling,[1] thermophotovoltaics,[2] infrared camouflage,[3] and thermal sources.[4,5] If the number and linewidth of resonance peaks inside a wide wavelength range could be reduced simultaneously, the unwanted radiation would be significantly minimized and then the energy utilization efficiency of thermal emitters would be improved. Therefore, simultaneous single-peak and narrowband thermal emitters are favored in many applications (such as sensing). The conventional strategy to realize a simultaneous single-peak and narrowband thermal emitter is to combine a high-temperature broad-band blackbody thermal source with an additional narrowband filtering element,[6] however, significant undesired radiation is simultaneously induced and the whole device is bulky. The recent development of micro- and nanophotonics has generated vigorous interest to deliberately tailor the absorption/emission spectrum over the mid-infrared region. Semiconductors,[7–9] metals,[10–17] and polar dielectrics[18–26] are three common types of materials in these studies.

For semiconductor-based emitters, the combination of intersubband transitions in multiple quantum wells and the photonic-crystal resonance effect allows for single-peak and narrowband emission; however, they still involve a complex fabrication process, and the emission peaks red-shift as the temperature rises due to the decrease in the intersubband absorption coefficiency at a higher temperature.[9] For metal-based emitters, various structures have been adopted: (i) for metal-insulator-metal structures,[11–13] the inherent high optical loss of metals in the mid-infrared range makes it difficult to achieve narrowband emission;[27] (ii) for metallic gratings and bull's eye structures,[10,17] narrowband emission could be obtained through Bragg resonance. However, their peak emissivity is not high (<0.7); (iii) for tamm plasmon polaritons structures,[15,16] they exhibit narrowband emission, but the total thickness is quite large (approximately micrometers) since multilayers are adopted, rendering these emitters bulky. Polar dielectrics (such as SiC), which support surface phonon polaritons (SPhPs) through the interactions between the incident electromagnetic radiation and the intrinsic vibrations of optical phonons, act like metals inside the Reststrahlen band [from the longitudinal optical (LO) phonon mode to the transverse optical (TO) phonon mode].[27,28] The optical phonons possess relatively long lifetimes (approximately

picoseconds) and polar dielectrics thereby exhibit comparatively low optical loss (including gratings,[18–20] antennas,[21–24] and metasurfaces[25,26]). Narrowband thermal emission with SiC gratings has been demonstrated.[18] However, multiple peaks at the edge of the Reststrahlen band are introduced (see Fig. S1 for the emission of SiC gratings), thus degrading the energy-efficiency in comparison with a single-peak emitter at a target emission wavelength at the same input power/energy.[7] Therefore, the development of simultaneous single-peak and narrowband thermal emitters with the merits of a simple configuration and ease-of-fabrication, which emit radiation at a narrow wavelength range and restrain radiation at other wavelengths, remains a challenge.

In this paper, we demonstrate simultaneous single-peak and narrowband thermal radiation with the merits of a simple configuration and ease-of-fabrication by hybridizing the metal structure with the polar dielectric. The metal provides the single-peak emission in a broad spectrum range and the polar dielectric assists the narrowband operation. The emitter is composed of a one-dimensional array of gold strips onto a polar dielectric SiC substrate. This emitter presents several distinct features: (i) single-peak emission between 2.5 μm and 25 μm with a peak emissivity up to 0.94 at 11.2 μm wavelength for TM (transverse magnetic) polarization, which is dominated by a hybrid plasmon/phonon mode; (ii) narrow bandwidth with a quality factor of 19; (iii) simple configuration with a layer of one-dimensional metal structures; and (iv) high-temperature endurance (at least 600 °C) if the metallic array is composed of molybdenum. This emitter may pave the way toward plenty of energy-efficient applications including thermal sources, thermophotovoltaics, and sensing.

This emitter consists of a one-dimensional array of Au microstrips on an SiC substrate [Fig. 1(a)]. Each unit cell consists of a gold microstrip with the height (h) of 280 nm. The gap size (g) between every two Au strips is 1.6 μm. The period (p) is 7.3 μm [Figs. 1(b) and 1(c), see the supplementary material Note 1 for the sample fabrication]. The electric field E is along the y and x axes for TE and TM polarized light, respectively. The refractive indices of Mo, Au,[5] and SiC[29] are derived from an ellipsometer and the literature, respectively (Fig. S2). Within the wavelength range (termed as the Reststrahlen band) between LO and TO phonon wavelengths of SiC (10.32 μm and 12.61 μm, respectively), the real part (n) of the refractive index is much smaller than the imaginary part (k), the calculated absorptivity and measured emissivity spectra of SiC are given in Fig. S3.

Experimental emission intensity spectra of the blackbody and Au/SiC with TM polarization at different temperatures (from 100 to 380 °C) are presented in Fig. 2(a). Apparently, the blackbody emission maintains at a high level over a broad wavelength range with a low quality factor [$\lambda_0/\Delta\lambda$, λ_0 is the peak wavelength and $\Delta\lambda$ is the full width at half-maximum (FWHM)]. With the hybrid Au/SiC structure,

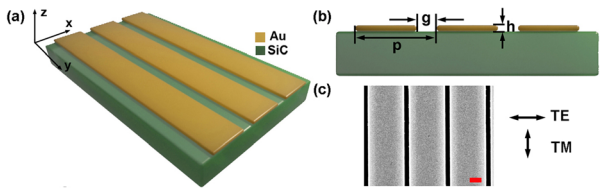

FIG. 1. (a) Schematic diagram and (b) cross-sectional view of the emitter. (c) SEM top-view image of the fabricated structure. The scale bar is 2 μm. The arrows indicate the TE and TM polarization, respectively.

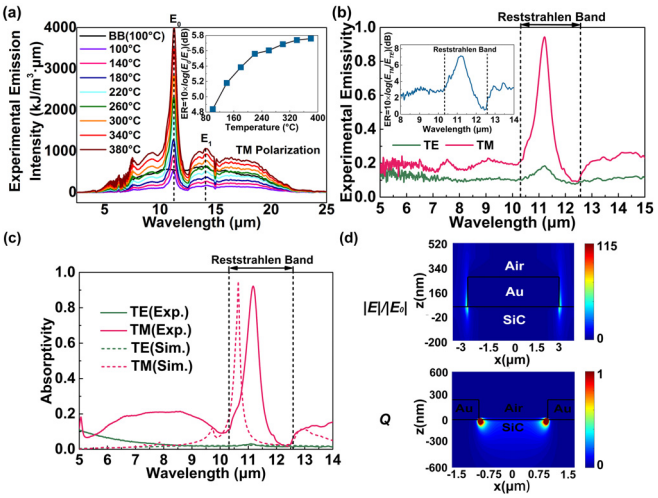

FIG. 2. (a) Measured TM-polarized emission intensity spectra of the blackbody and Au/SiC from the normal direction. The black line is for the blackbody (black soot) at 100 °C. Other lines are for the sample at different temperatures. The inset is the extinction ratio between E_0 at 11.2 μm and E_1 at 14.1 μm. (b) Measured emissivity spectra of Au/SiC at 100 °C from the normal direction with TE and TM polarized light. The inset is the extinction ratio of between TM and TE polarized emissions. (c) Measured (solid lines) and calculated (dashed lines) absorptivity spectra of Au/SiC under normal incidence with TE and TM polarized light. (d) Electric field enhancement ($|E/E_0|$, E_0 is the incident electric field, top) and resistive loss (Q, bottom) distribution at the simulated resonance wavelength of 10.6 μm under TM polarization.

the thermal emission can be tailored with an emission peak at the resonance of 11.2 μm, while at other wavelengths it is suppressed. By increasing the device temperature, the emission peak of this emitter shows a rising trend at the resonance, which implies that the power of this emitter can be enhanced by heating the device. Apart from the emission peak at 11.2 μm, weak emission at around 14.1 μm also can be seen. To clearly demonstrate the radiation suppression property, we define the extinction ratio between the emissivity (E_0) at 11.2 μm and 14.1 μm (E_1) as $ER = 10 \times \log(E_0/E_1)$ [inset of Fig. 2(a)]. When the temperature changes from 100 °C to 380 °C, the extinction ratio remains over 4.8 dB. The experimental polarization-dependent emissivity spectra are shown in Fig. 2(b). The maximum emissivity of this hybrid Au/SiC structure for TM polarization is 0.94 at the resonance of 11.2 μm, while for TE polarization, the emissivity is less than 0.2 across all the wavelengths we measured. For TM polarization, the FWHM of the peak is 0.6 μm, implying a quality factor of 19. The corresponding extinction ratio for these two polarizations [$ER = 10 \times \log(E_{TM}/E_{TE})$, E_{TM} and E_{TE} are the measured emissivities of Au/SiC at the same wavelength under TM and TE polarization, respectively] is as large as 7.1 dB [inset of Fig. 2(b)].

The absorption property of the Au/SiC emitter was calculated by the COMSOL Multiphysics software [Fig. 2(c)]. According to Kirchhoff's law of thermal radiation, the values of absorptivity and emissivity of an object at any wavelength are the same. The experimental emissivity and absorptivity under TE and TM polarization conform to this rule [Figs. 2(b) and 2(c)]. The red-shift of resonance indicates that ν_{LO} is larger than the simulation while the resonance broadening is caused by additional loss including the material loss of

SiC and scattering loss owing to the fabrication imperfection. Emission, emissivity, and absorptivity measurements can refer to the supplementary material Note 1. To study the angular dependence, mid-infrared absorptivity spectra are acquired by illuminating the samples with TM-polarized light at various incident angles (Fig. S4). Single-peak absorption is apparent for an incident angle of less than 30°, with a maximum absorptivity over 0.66. The calculated electric field enhancement ($|E|/E_0|$) and resistive loss (Q, see the supplementary material Note 2) distributions manifest a hybrid plasmon/phonon mode [Fig. 2(d)]. The maximum electric field enhancement (~115) occurs at the corners of the bottom of Au strips (air/Au/SiC). To show the necessity for employing a metal/SiC structure for simultaneous single-peak and narrowband emission, the TM-polarized absorption/emission properties of SiC/SiC, SiC/Au and Au/SiC structures were calculated (see the supplementary material Note 3).

Increasing the working temperature of thermal emitters could improve the radiated power. Therefore, investigating the long-term thermal stability of thermal emitters at a high temperature is essential for practical applications. Noble metals have low melting points,[30] restricting their usage under some high temperature conditions. A few refractory materials (e.g., Mo, W, TiN, and SiC) have been selected as better replacements for noble metals.[10,11,17,30,31] We initially baked the Au/SiC emitter at 600 °C for 30 min by a rapid thermal processing furnace. A slight resonance wavelength shift from 11.2 μm to 11.0 μm can be seen, but the single-peak emission still exists with the peak emissivity beyond 0.90 after 30 min heating [Fig. 3(a)]. Some large-sized grains on the Au surfaces were generated due to the low melting point of Au microstructures [Fig. 3(c)]. This will lead to the deformation of the Au arrays and deteriorate the radiation performance of this emitter. Therefore, the maximum endurable operating temperature of the Au/SiC emitter is below 600 °C.

To improve the thermal endurance, we choose Mo as a substitute for Au [inset of Fig. 3(b)], as Mo and Au share similar optical properties in the mid-infrared regime (Fig. S2). The single-peak emissivity is 0.87 at the wavelength of 11.1 μm [Fig. 3(b)]. The emissivity of the Mo/SiC structure can be improved by optimizing the fabrication (e.g., replacing photolithography by e-beam lithography). This Mo/SiC emitter still retains its emission performance after baking under the same conditions. The Mo grains still retain their shapes throughout the heating process, which ensures the emission stability of this Mo/SiC thermal device [Fig. 3(d)]. Hence, we can conclude that this Mo/SiC emitter could withstand at least 600 °C for 30 min, which is desirable for operation in some high temperature environments (e.g., gas reaction environment).

To manifest the single-polarized thermal emission property of the Au/SiC structure, the spatial emission performances of patterned Au/SiC structures are further investigated. The spatial information can be "encrypted" by patterning the top Au array with different directions. Here, we fabricated two samples: strip and checkerboard pattern (Fig. 4). The Au arrays of every single adjacent area are mutually perpendicular to each other (area I and II). For both strip (S1) and checkerboard (S2) patterns, the smallest linewidth is the same (3 mm), with the total area of around $12 \times 12\,mm^2$ and $12 \times 9\,mm^2$, respectively. The sample is placed onto a heating stage at the temperature of 100 °C, with an infrared camera mounted above. The infrared camera captures the spatial power in the 8–14 μm wavelength range. The radiation temperature (T_r) on the scale bar is related to the total received power (P_{tot}). The infrared images for these two samples are initially captured without a polarizer [Figs. 4(a) and 4(b)]. The radiation temperature is uniform for the Au/SiC structure (areas I and II). After

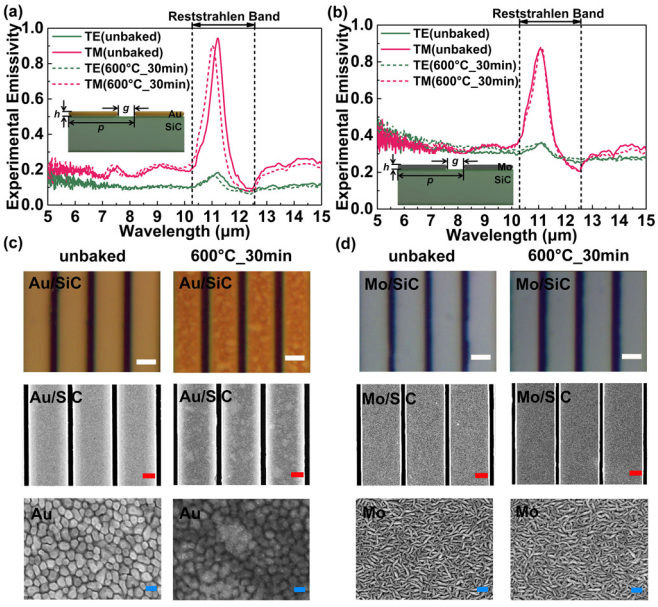

FIG. 3. Measured emissivity spectra of (a) Au/SiC and (b) Mo/SiC before and after baking. The results are obtained under TE and TM polarized normal incident light, respectively. Optical microscopy and SEM images of (c) Au/SiC and (d) Mo/SiC before and after baking. The first row is the optical microscope images (white scale bar: 10 μm). The second row is the magnified view of SEM images (red scale bar: 2 μm). The third row is the wider view of SEM images (blue scale bar: 100 nm). Inset of (b) shows the cross-sectional schematic diagram of Mo/SiC ($p = 7\,\mu$m, $g = 2\,\mu$m, $h = 250$ nm), which is similar to Au/SiC ($p = 7.3\,\mu$m, $g = 1.6\,\mu$m, $h = 280$ nm) in (a).

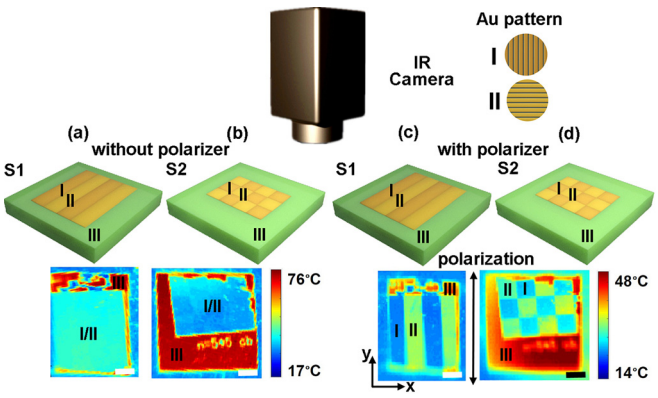

FIG. 4. Infrared images of (a) S1 without the polarizer, (b) S2 without the polarizer, (c) S1 with the polarizer, and (d) S2 with the polarizer. The arrow in (c) and (d) denotes the direction of the polarizer. The color bars on the right represent the radiation temperature recorded by the camera. The scale bar is 3 mm. S1 and S2 are the strip and checkerboard patterns of the Au arrays onto SiC substrates, respectively. On the top are simple schematic diagrams of the setups for capturing the infrared images. For areas I and II, the directions of Au arrays are mutually perpendicular, which is depicted by different colors. Area III represents the SiC.

inserting a polarizer (aligned with the y-axis), the total captured power by the camera is reduced for both area I and II as only y-polarized radiation can pass through the polarizer [Figs. 4(c) and 4(d)]. The radiation temperature for area I is lower than that for area II. Area III (bare SiC) always shows the highest radiation temperature. The total power (P_{tot}) captured by the camera is related to two parts—emitted radiation power of the sample (P_{emit}) and reflected radiation power of the environment (P_{ref}) (see the supplementary material Note 4). The calculated power captured by the camera for different areas (I, II, and III) before and after inserting the polarizer (y-polarized) can be found in Table S1. Before inserting the polarizer, the calculated P_{tot} for bare SiC (area III) is 643.2 W m^{-3}, which mainly comes from the emitted power by SiC itself (accounting for 74%). The calculated P_{tot} for Au/SiC is 440.6 W m^{-3}, which mainly comes from the reflected radiation power of the environment (accounting for 63%). After inserting the polarizer, the calculated P_{tot} for areas I and areas II are 200.6 W m^{-3} and 240.0 W m^{-3}, respectively, indicating higher radiation temperature for area II.

In conclusion, we introduced a hybrid metal/polar dielectric structure to realize a simultaneous single-peak and narrowband thermal emitter with the merits of a simple configuration and ease-of-fabrication. This emitter consists of a 280-nm-thick gold structure on the SiC polar dielectric substrate. The metal provides the single-peak emission in a broad spectrum range and the polar dielectric assist the narrowband operation. The near-unity single-peak emissivity is based on a hybrid plasmon/phonon mode under TM polarization. For the hybrid Au/SiC structure, the narrowband emission has a quality factor of 19 and thus helps to concentrate the total input thermal energy into the narrowband emission window. The thermal stability of this hybrid metal/polar dielectric structure is enhanced by employing a refractory material Mo. This device shows great potential in numerous energy-efficient applications including gas sensing, thermal sources, and thermophotovoltaics.

See the supplementary material for a complete description of the experimental methods, resistive loss, comparison between different structures, power calculation, and additional data.

This work was supported by the National Key Research and Development Program of China (No. 2017YFA0205700), the National Natural Science Foundation of China (Grant Nos. 61425023, 61575177, and 61775194), and the Fundamental Research Funds for the Central Universities.

REFERENCES

[1]A. P. Raman, M. A. Anoma, L. Zhu, E. Rephaeli, and S. Fan, Nature **515**, 540 (2014).
[2]A. Lenert, D. M. Bierman, Y. Nam, W. R. Chan, I. Celanović, M. Soljačić, and E. N. Wang, Nat. Nanotechnol. **9**, 126 (2014).
[3]Y. Qu, Q. Li, L. Cai, M. Pan, P. Ghosh, K. Du, and M. Qiu, Light Sci. Appl. **7**, 26 (2018).
[4]Y. Qu, Q. Li, K. Du, L. Cai, J. Lu, and M. Qiu, Laser Photonics Rev. **11**, 1700091 (2017).
[5]K. Du, L. Cai, H. Luo, Y. Lu, J. Tian, Y. Qu, P. Ghosh, Y. Lyu, Z. Cheng, M. Qiu, and Q. Li, Nanoscale **10**, 4415 (2018).
[6]O. Ilic, P. Bermel, G. Chen, J. D. Joannopoulos, I. Celanović, and M. Soljacič, Nat. Nanotechnol. **11**, 320 (2016).
[7]M. D. Zoysa, T. Asano, K. Mochizuki, A. Oskooi, T. Inoue, and S. Noda, Nat. Photonics **6**, 535 (2012).
[8]Q. Li, J. Lu, P. Gupta, and M. Qiu, Adv. Opt. Mater. **7**, 1900595 (2019).
[9]T. Inoue, M. D. Zoysa, T. Asano, and S. Noda, Appl. Phys. Lett. **108**, 0911019 (2016).
[10]J. Liu, U. Guler, A. Lagutchev, A. Kildishev, O. Malis, A. Boltasseva, and V. M. Shalaev, Opt. Mater. Express **5**, 2721 (2015).
[11]T. Yokoyama, T. D. Dao, K. Chen, S. Ishii, R. P. Sugavaneshwar, M. Kitajima, and T. Nagao, Adv. Opt. Mater. **4**, 1987 (2016).
[12]X. Liu, T. Tyler, T. Starr, A. F. Starr, N. M. Jokerst, and W. J. Padilla, Phys. Rev. Lett. **107**, 045901 (2011).
[13]B. Liu, W. Gong, B. Yu, P. Li, and S. Shen, Nano Lett. **17**, 666 (2017).
[14]J. Zhou, X. Chen, and L. J. Guo, Adv. Mater. **28**, 3017 (2016).
[15]H. Zhu, H. Luo, Q. Li, D. Zhao, L. Cai, K. Du, Z. Xu, P. Ghosh, and M. Qiu, Opt. Lett. **43**, 5230 (2018).
[16]Z. Wang, J. K. Clark, Y. L. Ho, B. Vilquin, H. Daiguji, and J. J. Delaunay, ACS Photonics **5**, 2446 (2018).
[17]J. H. Park, S. E. Han, P. Nagpal, and D. J. Norris, ACS Photonics **3**, 494 (2016).
[18]J. J. Greffet, R. Carminati, K. Joulain, J. P. Mulet, S. Mainguy, and Y. Chen, Nature **416**, 61 (2002).
[19]J. L. Gall, M. Olivier, and J. J. Graffet, Phys. Rev. B **55**, 10105 (1997).
[20]W. Streyer, S. Law, A. Rosenberg, C. Roberts, V. A. Podoiskiy, A. J. Hoffman, and D. Wasserman, Appl. Phys. Lett. **104**, 131105 (2014).
[21]T. Wang, P. Li, D. N. Chigrin, A. J. Giles, F. J. Bezares, O. J. Glembocki, J. D. Caldwell, and T. Taubner, ACS Photonics **4**, 1753 (2017).
[22]J. A. Schuller, T. Taubner, and M. L. Brongersma, Nat. Photonics **3**, 658 (2009).
[23]Y. Chen, Y. Francescato, J. D. Caldwell, V. Giannini, T. W. W. Maß, O. J. Glembocki, F. J. Bezares, T. Taubner, R. Kasica, M. Hong, and S. A. Maier, ACS Photonics **1**, 718 (2014).
[24]A. D. Dunkelberger, C. T. Ellis, D. C. Ratchford, A. J. Giles, M. Kim, C. S. Kim, B. T. Spann, I. Vurgaftman, J. G. Tischler, J. P. Long, O. J. Glembocki, J. C. Owrutsky, and J. D. Caldwell, Nat. Photonics **12**, 50 (2018).
[25]Y. Yang, S. Taylor, H. Alshehri, and L. Wang, Appl. Phys. Lett. **111**, 051904 (2017).
[26]X. Zhang, H. Liu, Z. G. Zhang, Q. Wang, and S. N. Zhu, Sci. Rep. **7**, 41858 (2017).
[27]J. D. Caldwell, L. Lindsay, V. Giannini, I. Vurgaftman, T. L. Reinecke, S. A. Maier, and O. J. Glembocki, Nanophotonics **4**, 44 (2015).
[28]P. Li, X. Yang, T. W. W. Maβ, J. Hanss, M. Lewin, A. K. U. Michel, M. Wutting, and T. Taubner, Nat. Mater. **15**, 870 (2016).
[29]L. Cai, K. Du, Y. Qu, H. Luo, M. Pan, M. Qiu, and Q. Li, Opt. Lett. **43**, 1295 (2018).
[30]W. Li, U. Guler, N. Kinsey, G. V. Naik, A. Boltasseva, J. Guan, V. M. Shalaev, and A. V. Kildishev, Adv. Mater. **26**, 7959 (2014).
[31]I. Ohdomari, S. Sha, H. Aochi, T. Chikyow, and S. Suzuki, J. Appl. Phys. **62**, 3747 (1987).